Aging behavior of spin glasses under bond and temperature perturbations from laser illumination

Ryuta Arai, Katsuyoshi Komatsu, and Tetsuya Sato
Department of Applied Physics and Physico-Informatics, Keio University, 3-14-1 Hiyoshi, Kohoku-ku, Yokohama-shi, Kanagawa 223-8522, Japan
(Received 6 January 2007; published 23 April 2007)

We have studied the nonequilibrium dynamics of spin glasses subjected to bond perturbation, which was based on the direct change in the spin-spin interaction ΔJ, using photoillumination in addition to temperature change ΔT. Differences in time-dependent magnetization are observed between that under $\Delta T+\Delta J$ and ΔT perturbations with the same ΔT. These differences show the contribution of ΔJ to spin-glass dynamics through the decrease in the overlap length. That is, the overlap length $L_{\Delta T+\Delta J}$ under $\Delta T+\Delta J$ perturbation is less than $L_{\Delta T}$ under ΔT perturbation. Furthermore, we observe the crossover between weakly and strongly perturbed regimes under bond cycling accompanied by temperature cycling. These effects of bond perturbation strongly indicate the existence of both chaos and the overlap length.

DOI: 10.1103/PhysRevB.75.144424 PACS number(s): 75.50.Lk, 75.50.Pp, 75.40.Gb

I. INTRODUCTION

Spin glasses have been studied for the past several decades, but many questions about the nonequilibrium dynamics of spin glasses still remain. To clarify the nature of spin glass below the transition temperature, the aging behavior[1] in the relaxation of magnetization in spin glasses has been actively studied. Especially the aging of spin glasses subjected to perturbations ΔX, such as changes in temperature ΔT and in bond interaction ΔJ, has been extensively studied because it shows characteristic behaviors peculiar to spin glasses, such as memory and rejuvenation.[2,3] These behaviors were interpreted in terms of the phenomenological scaling theory, called the droplet model.[4–6] According to this theory, the memory and rejuvenation effects are explained in terms of the concept of chaos accompanied by the overlap length $L_{\Delta X}$.[4,6] The correlation between two equilibrium states, before and after the perturbation, disappears at the length scale L beyond the overlap length $L_{\Delta X}$. However, the chaotic nature appears even at weak perturbation ΔX, which satisfies $L<L_{\Delta X}$.[7–9] At strong perturbation ΔX, which satisfies $L>L_{\Delta X}$, the aging effect before the perturbation is not easily removed, but the memory effect is observed. These contradictory aspects can be explained based on the ghost domain scenario.[7,10–12] Thus, the crossover between a weakly perturbed regime ($L<L_{\Delta X}$) and a strongly perturbed regime ($L<L_{\Delta X}$) (Refs. 11 and 12) should be clarified so that we can gain an intrinsic understanding of the rejuvenation and memory effects based on the droplet picture.

So far, the experimental studies[12–16] and simulations[17–19] of spin glasses have been conducted exclusively under the temperature cycling protocol. In such an experimental protocol based on temperature change, however, this change inevitably affects the thermal excitation of the droplet and thus leads to strong separation of the time scales.[10] This makes it difficult to demonstrate the existence temperature chaos. In fact, several papers[18–21] claim that the rejuvenation-memory effects observed in temperature cycling can be attributed to the differences among the length scales caused by the change in temperature. If the *direct* change in the bond, ΔJ, can be used in this kind of experiment without the change in time scales, it is expected that the chaotic effect and the overlap length could be more clearly analyzed.

The direct change in the spin-spin interaction ΔJ can be realized through the photoexcitation of carriers using a semiconductor spin glass: e.g., $Cd_{1-x}Mn_xTe$.[22–25] The relaxation in thermoremanent magnetization and that in isothermal remanent magnetization of $Cd_{1-x}Mn_xTe$ were observed under unpolarized light illumination.[26] Recently, we studied the aging behavior of $Cd_{1-x}Mn_xTe$ under photoillumination and showed that the ΔJ contribution can be deduced by comparing the data under $\Delta T+\Delta J$ and ΔT perturbations with the same ΔT.[27] To date, however, there has been no systematic study of the aging behavior under bond perturbation. It is essential to obtain evidence of the existence of the chaotic effect and of the change in the overlap length expected in the droplet model[4,5] through the analysis of bond perturbation data.

In this study we first confirm that bond perturbation using photoillumination affects the spin-glass dynamics. We estimated that $\Delta J\sim 0.14$—0.40 K at $\Delta T=0.26$ K. The second purpose is to clarify the characteristics of overlap length and to specify the crossover between weakly and strongly perturbed regimes to demonstrate the validity of the droplet picture.

II. EXPERIMENTAL DETAILS

The sample was a single crystal of $Cd_{0.63}Mn_{0.37}Te$ (band gap energy $E_g=2.181$ eV), which was prepared using the vertical Bridgman technique. The magnetization of the sample, which was a plate 1.2 mm thick, was measured by a Quantum Design MPMS5 superconducting quantum interference device (SQUID) magnetometer. Figure 1 shows the temperature-dependent magnetization under field-cooled (FC) and zero-field-cooled (ZFC) conditions in $H=100$ Oe.[29] The spin-freezing temperature $T_f\sim 10.7$ K was evaluated. Light was guided to the sample through a quartz optical fiber so as to be parallel to an external magnetic field. The light source was a green He-Ne laser with $\lambda=543.5$ nm (2.281 eV), where this photon energy was slightly larger than the band gap energy of the sample. One side of the

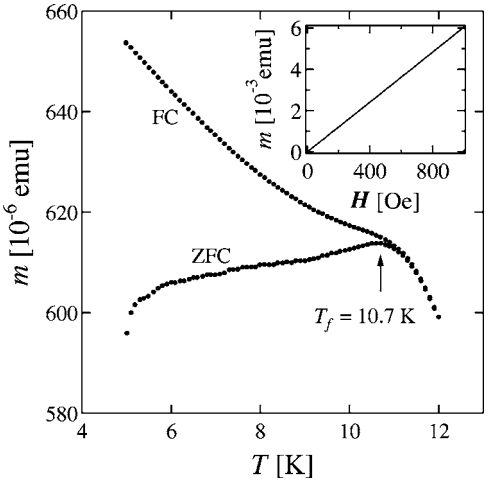

FIG. 1. Temperature dependence of ZFC and FC magnetizations of $Cd_{0.63}Mn_{0.37}Te$ in $H=100$ Oe. The freezing temperature of ~10.7 K estimated by this graph. The inset shows the field dependence of the magnetization at 7 K ($=T_m$).

sample was coated with carbon. If light was illuminated on the carbon-coated side, the light was absorbed in a carbon blackbody and thus only the thermal contribution ΔT appeared. When the light was illuminated on the opposite side, a change in the bond interaction, ΔJ, appeared in addition to ΔT.[28] We determined the sample temperature during the illumination based on the change in field-cooled magnetization as shown in Fig. 1. The photoinduced magnetization in $Cd_{0.63}Mn_{0.37}Te$ was scarcely observed (less than 0.01 of the total magnetization change by the photo illumination),[28] and thus we were able to neglect it. The light intensity was adjusted so as to obtain the same increment of sample temperatures under both the illumination conditions. This made it possible to consider only the ΔJ contribution by comparing the $\Delta T+\Delta J$ data with the ΔT data. We note that the change in temperature by the illumination was given to a sample with steplike heating and cooling.[28] Thus we could also neglect the effect of the finite cooling/heating rate.[12,17]

The time dependence of magnetization was measured according to the following procedure (Fig. 2). The sample was zero-field-cooled down to T_m as rapidly as possible (~10 K/min) from 30 K which is above the transition temperature T_g. Then, the temperature T_m was held for t_w (=3000 s) (initial aging stage). After that, the perturbation was given to the sample during t_p using the photoillumination (perturbation stage). After the light was turned off, a magnetic field H of 100 Oe, at which the linear field-dependent magnetization was held (inset of Fig. 1), was subsequently applied. After $t_s \sim 60$ s, the magnetic field H of 100 Oe is stabilized, and then the magnetization M was measured as a function of time t (healing stage).

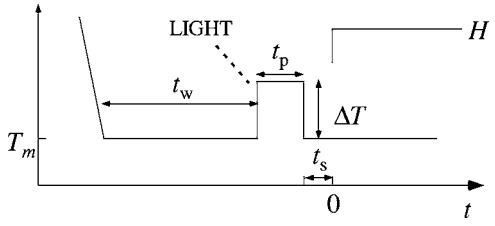

FIG. 2. Experimental protocol of bond-cycling process under photoillumination. The sample was first cooled to $T_m=7$ K and aged during $t_w=3000$ s (initial aging stage). The perturbation was subsequently added during t_p (perturbation stage) using photoillumination. After the perturbation was stopped, H of 100 Oe was applied and the magnetization was measured as a function of t (healing stage).

The dynamics of a spin glass below T_g is governed by excitations of the droplet.[4] The size $L_{T_m}(t)$ of the droplet, which was thermally activated at T_m within the time scale t, is given by the following equation:[4]

$$L_{T_m}(t) \sim L_0\left[\frac{k_B T_m \ln(t/\tau_0)}{\Delta(T_m)}\right]^{1/\psi}. \quad (1)$$

Consequently, a significant difference in time scales existed even between two close temperatures T_m and $T_m+\Delta T$. Therefore, we define the effective duration $t_{\rm eff}(T_m)$ of the perturbation[10] according to

$$L_{T_m+\Delta T}(t_p) = L_{T_m}(t_{\rm eff}) \quad (2)$$

or

$$t_p(T_m+\Delta T) = \tau_0[t_{\rm eff}(T_m)/\tau_0]^{T_m/(T_m+\Delta T)}, \quad (3)$$

where τ_0 ($\sim\hbar/J\sim 10^{-13}$ s) is a microscopic time scale.[30] When we discuss the data below, we convert the actual duration of the perturbation $t_p(T_m+\Delta T)$ into the effective duration $t_{\rm eff}(T_m)$.

III. EXPERIMENTAL RESULTS

We focused on the relaxation rate of the magnetization, $S=(1/H)dM/d\ln t$, measured under the various conditions of strength and duration of the perturbation. Since we observed the peaks in the perturbation time-dependent data of S, the height of each peak and the corresponding peak position are important for our discussion.

The solid curves in Fig. 3 show the time dependence of the relaxation rate S, measured after the aging time $t_w=3000$ s without illumination (isothermal aging). These curves show a peak at $t\sim 3000$ s, which is a typical behavior observed in many spin glasses.[31]

Figure 3 also shows the typical data of perturbation time-dependent S at T_m (=7 K) of the sample, where the constant temperature increment ΔT (=0.26 K, 1.05 K) is added during $t_{\rm eff}$ for the perturbation. The left figures [(a) and (c)] and the right figures [(b) and (d)] show the data under ΔT and $\Delta T+\Delta J$ perturbations, respectively. All the data are normalized by the maximum height of S without photoillumination. In Figs. 3(a) and 3(b) ($\Delta T=0.26$ K), the peak in S at $t\sim t_w$ (we call this the *main peak*) becomes gradually depressed compared with the isothermal aging curve as $t_{\rm eff}$ increases. The depression of S in Fig. 3(b) is more pronounced than that in Fig. 3(a) at the same $t_{\rm eff}$. In addition, the peak position in the main peak shifts to a longer time as $t_{\rm eff}$ increases in both Figs. 3(a) and 3(b). In Figs. 3(c) and 3(d)

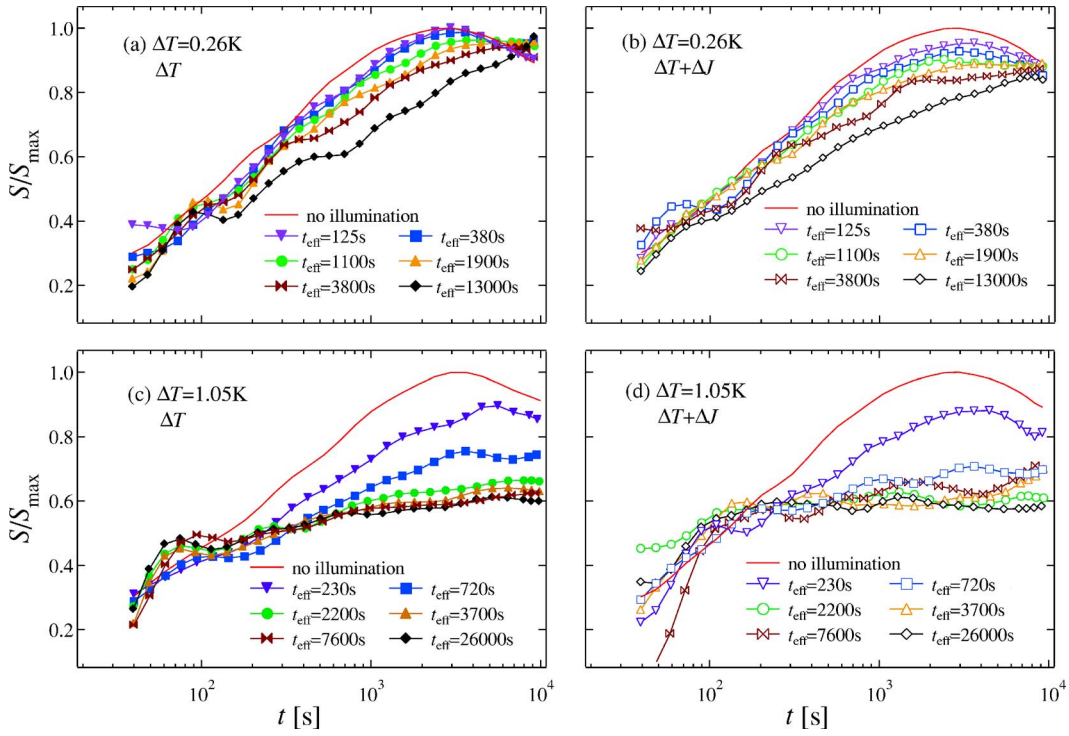

FIG. 3. (Color online) Time dependence of the relaxation rate S at 7 K. Solid curves show S, measured after the waiting time $t_w=3000$ s without illumination (isothermal aging). (a) (solid symbols) and (b) (open symbols) show the relaxation rates S at various t_{eff} for $\Delta T=0.26$ K under ΔT and $\Delta T+\Delta J$ perturbations, respectively. (c) (solid symbols) and (d) (open symbols) show the relaxation rates S at various t_{eff} for $\Delta T=1.05$ K under ΔT and $\Delta T+\Delta J$ perturbations, respectively. All the data are normalized by the maximum height of S without photoillumination.

($\Delta T=1.05$ K), the main peak in S is depressed with increasing t_{eff} in a more pronounced way compared with the data at $\Delta T=0.26$ K. For long t_{eff}, S becomes almost flat, but the main peak is incompletely erased. Furthermore, in Figs. 3(c) and 3(d), a small peak appears around $t\sim 100$ s (we call this the *subpeak*) except for short t_{eff}, and the subpeak becomes more pronounced with increasing t_{eff}. The subpeak in Fig. 3(d) is less sensitive to t_{eff} compared with that in Fig. 3(c). In Fig. 3(d), the subpeak is so close to the main peak that the two peaks are insufficiently separable. We note that some curves in S in Fig. 3 show a sudden increase at large values of t [e.g., S for $t_{eff}\sim 7600$ s in Fig. 3(d) ($\bowtie$symbols)]. This may be due to a small fluctuation in the sample temperature.

IV. DISCUSSION

A. Theory based on the ghost domain scenario

Recently, the aging behavior under the bond or temperature cycle has been explained based on the behavior of domains in terms of the ghost domain picture.[10–12] In the following paragraphs, we interpret our results based on the behavior of the domain under the bond or temperature cycle in the same way. We divide our experimental protocol into three stages according to Fig. 2: the initial aging stage in which the equilibrium state Γ_A belongs to the environment $A-(T_m,J)$, the perturbation stage in which the equilibrium state Γ_B belongs to the new environment $B-(T_m+\Delta T,J+\Delta J)$, and the healing stage at the environment A.

In the initial aging stage, the domains belonging to Γ_A at T_m grow during t_w according to Eq. (1). In the perturbation stage, the perturbation ΔX (ΔT or $\Delta T+\Delta J$) is applied from t_w to t_w+t_p. During the perturbation stage, the "overlap" between the equilibrium states Γ_A and Γ_B disappears at the length scale beyond the overlap length $L_{\Delta X}$. The relation between $L_{\Delta X}$ and the perturbation ΔX is given as[4,6]

$$L_{\Delta X}=L_0|\Delta X/J|^{-1/\zeta}. \tag{4}$$

The chaos exponent ζ is given by $\zeta=d_s/2-\theta(>0)$, where d_s is a fractal dimension and θ is a stiffness exponent. Theoretically, temperature and bond perturbations are equivalent with respect to the overlap length $L_{\Delta X}$.[11]

We can distinguish the weakly and strongly perturbed regimes based on the relationship between overlap length $L_{\Delta X}$ and the domain size grown during each stages.[11,12] If $L_{T_m+\Delta T}(t_p)<L_{\Delta X}$, a weakly perturbed regime appears, in which the rejuvenation scarcely emerges.[9] If all the $L_{T_m}(t_w)$, $L_{T_m+\Delta T}(t_p)$, and $L_{T_m}(t)$ are greater than $L_{\Delta X}$, a strongly perturbed regime appears, in which the initial spin configuration is unstable with respect to droplet excitation and a new equilibrium state appears. This suggests a chaotic nature. The chaos, however, does not appear abruptly,[7,8] and there exists a crossover between the weakly and strongly perturbed regimes.

In the weakly perturbed regime, the domain belonging to Γ_A is weakly modified and the order parameter ρ slowly decreases in the perturbation stage. The order parameter in

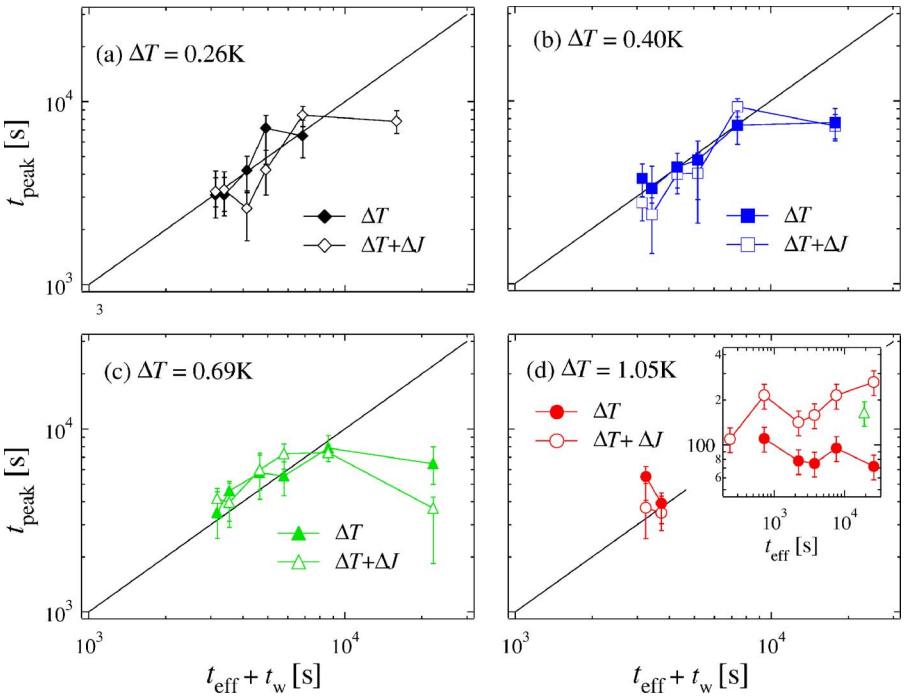

FIG. 4. (Color online) The $t_{\mathrm{eff}}+t_{\mathrm{w}}$ dependent t_{peak} at various values of ΔT. The increments of temperature under photoillumination, ΔT, are 0.26, 0.40, 0.69, and 1.05 K. The solid lines satisfies the equation $t_{\mathrm{peak}}=t_{\mathrm{w}}+t_{\mathrm{eff}}$. Solid symbols and open symbols show t_{peak} under ΔT and $\Delta T+\Delta J$ perturbations, respectively. The inset shows t_{eff}-dependent t'_{peak}. The symbols in the inset correspond to those in the main frame.

the domains is easily recovered during the healing stage. Thus, the recovery time τ_{rec}, which is necessary for the order parameter to saturate to 1, is given as

$$\tau_{\mathrm{rec}}^{\mathrm{weak}} \sim t_{\mathrm{eff}}. \tag{5}$$

In this regime, the size of domain belonging to Γ_A grows accumulatively so as to neglect the perturbation.

In the strongly perturbed regime, the spin configuration in domains belonging to Γ_A is completely random beyond the length scale of $L_{\Delta X}$ and the domains belonging to Γ_B grow during the perturbation stage. However, the effect of the initial domain of Γ_A remains as a ghost;[11,12] i.e., the domains, which grow up to $L_{T_m}(t_{\mathrm{w}})$ during initial aging, can vaguely keep their overall shapes (which are called *ghost domain*), and the domain interiors are significantly modified due to the growth of domains Γ_B. Thus, the order parameter ρ significantly decreases (but does not reach zero). When the perturbation is removed, the system recovers the initial spin configuration (healing stage). The recovery time τ_{rec} is given as

$$\tau_{\mathrm{rec}}^{\mathrm{strong}} \gg t_{\mathrm{eff}}. \tag{6}$$

In this regime, the domain belonging to Γ_A grows nonaccumulatively.

B. Role of the relaxation rate under the cycling

The relaxation rate S is characterized under the temperature or bond perturbations shown in Sec. IV A through the peak position and height in the time-dependent S. First, we define the characteristic time t_{peak} corresponding to the position of the main peak. The value of t_{peak} is shown as a function of $t_{\mathrm{eff}}+t_{\mathrm{w}}$ in Fig. 4(d) If the aging is accumulative, the spin configuration at $T_m+\Delta T$ in the perturbation stage is equivalent to that under the isothermal aging at T_m for t_{eff}. This results in the following relation:

$$t_{\mathrm{peak}} \sim t_{\mathrm{w}} + t_{\mathrm{eff}}, \tag{7}$$

which corresponds to the reference line in Fig. 4. In the strongly perturbed regime ($L \gg L_{\Delta X}$), on the other hand, the chaotic nature becomes effective and the position of the main peak shifts to a shorter time compared with the accumulative aging curve. In this case, t_{peak} satisfies the relation

$$t_{\mathrm{peak}} < t_{\mathrm{w}} + t_{\mathrm{eff}}. \tag{8}$$

During the healing stage, the order parameter of Γ_A starts to restore the domain structure grown during initial aging, and this is probably reflected in the height of the main peak. Thus, in order to characterize the change in the peak built in S, we define the relative peak height r, which is the ratio of the height in the main peak under the perturbation to that without perturbation. In other words, r is the measure of the memory after the perturbation.[12] The value of r is shown as a function of t_{eff} in Fig. 5.

In the completely weakly perturbed regime $[L_{T_m}(t_{\mathrm{eff}}) \ll L_{\Delta X}]$, the order parameter fully recovers at $t \sim t_{\mathrm{peak}}$ according to Eq. (5). However, close to the strongly perturbed regime (the crossover regime between the weakly and strongly perturbed regimes), the order parameter does not completely recover at $t=t_{\mathrm{w}}+t_{\mathrm{eff}}$. This leads to the decrease in the height of main peak. In the strongly perturbed regime, the order parameter insufficiently recovers because of the long recovery time $\tau_{\mathrm{rec}}^{\mathrm{strong}}$ given in Eq. (6). Thus, r is gradually depressed as t_{eff} increases because of the rapid increase in $\tau_{\mathrm{rec}}^{\mathrm{strong}}$. In addition, when the period t_{s} is necessary until the applied field is stabilized in a superconducting magnet after the perturbation is removed, the domain grows for t_{s} up to the size $L_{T_m}(t_{\mathrm{s}})$. This reflects the subpeak.[12] Thus, the subpeak becomes pronounced as the rejuvenation effects become clear.

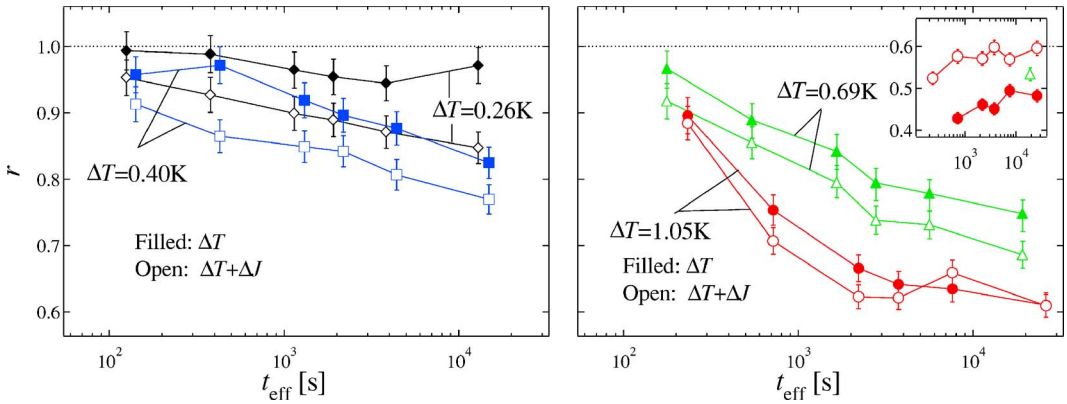

FIG. 5. (Color online) The $t_{\rm eff}$ dependent r at various values of ΔT. The increments of temperature under photo illumination, ΔT, are 0.26, 0.40, 0.69, and 1.05 K. The solid and open symbols show r under ΔT and $\Delta T+\Delta J$ perturbations, respectively. The inset shows $t_{\rm eff}$-dependent r'. The symbols in the inset correspond to those in the main frame.

C. Bond-cycling experiment

We try to classify our data, obtained under various perturbation conditions, into the following four categories: the weakly perturbed regime (we call this the *W* regime); the crossover regime, which is close to the weakly perturbed regime (we call this the *WC* regime); the crossover regime, which is close to the strongly perturbed regime (we call this the *SC* regime); and the strongly perturbed regime (we call this the *S* regime). The criteria for the classification are abridged in Table I. The classification is mainly performed based on Figs. 4 and 5 in which $t_{\rm peak}$ and r are arranged as a function of $t_{\rm eff}$ under various amplitudes of ΔT. The condition—i.e., $t_{\rm eff}$ be variable and ΔT be constant—corresponds to the situation that the domain size $L_{T_m}(t_{\rm eff})$ grown during the perturbation stage is variable while the overlap lengths $L_{\Delta T}$ and $L_{\Delta T+\Delta J}$ are constant. In addition, we also pay attention to the subpeak whose position and relative height are shown as $t'_{\rm peak}$ and r' in the insets in Figs. 4(d) and 5(b), respectively.

First we pay attention to the data at $\Delta T=0.26$ K under ΔT perturbation. As shown in Fig. 4(a), the values of $t_{\rm peak}$ almost merge into the reference curve except for the data at the longest $t_{\rm eff}+t_{\rm w}$, where the main peak for the longest $t_{\rm eff}$ should appear at time much longer than the present observation time window ($\sim$10 s). The subpeak cannot be observed, and r scarcely decreases from 1 (Fig. 5). Therefore, all the data at $\Delta T=0.26$ K under ΔT perturbation satisfy the criteria for the *W* regime in Table I. Thus, the accumulative aging proceeds in this condition.

Under the ΔJ perturbation in addition to $\Delta T=0.26$ K, the $t_{\rm peak}$ except for the longest $t_{\rm eff}$ satisfies Eq. (7) and the $t_{\rm peak}$, at the longest $t_{\rm eff}$, is shorter than $t_{\rm w}+t_{\rm eff}$ [Fig. 4(a)]. The value of r clearly decreases from 1 except for the shortest $t_{\rm eff}$ (Fig. 5). This indicates that the ΔJ perturbation decreases the overlap length according to Eq. (4). Under $\Delta T+\Delta J$ perturbation with $\Delta T=0.26$ K, thus, the system is *not* completely in the *W* regime, except for the shortest $t_{\rm eff}$, and the chaotic nature partially emerges. Thus, this regime is in the *WC* regime except for the shortest $t_{\rm eff}$, at which the system belongs to the *W* regime.

Under both perturbations with $\Delta T=0.40$ K [see Fig. 4(b)], the values of $t_{\rm peak}$ almost merge into the reference curve except for the data at the longest $t_{\rm eff}+t_{\rm w}$. At the longest $t_{\rm eff}+t_{\rm w}$, the values of $t_{\rm peak}$ under both perturbations merge together, but lie below the reference curve. Under the ΔT perturbation, r is clearly lower than 1 except for the small $t_{\rm eff}$, while r under the $\Delta T+\Delta J$ perturbation it is clearly lower than 1 over the entire range of $t_{\rm eff}$ (Fig. 5). The subpeak cannot be observed under either perturbation. Therefore, at $\Delta T=0.40$ K under the ΔT perturbation, the system belongs to the *WC* regime except for short $t_{\rm eff}$, at which the system belongs to the *W* regime. Under the $\Delta T+\Delta J$ perturbation, the system belongs to the *WC* regime.

Next, we turn to the data under the strongest perturbation ($\Delta T=1.05$ K) prior to the discussion of complex behavior under the medium perturbation ($\Delta T=0.69$ K). At $\Delta T=1.05$ K, $t_{\rm peak}$ cannot be determined at $\Delta T=1.05$ K because the *S* curves are so flattened except for the short $t_{\rm eff}$ [see Fig. 4(d)]. The value of r rapidly decreases as $t_{\rm eff}$ increases and becomes almost constant in the long-$t_{\rm eff}$ region, in which r under both perturbations merge (Fig. 5). The subpeak under the ΔT perturbation is observed except for the shortest $t_{\rm eff}$ and becomes pronounced with increasing $t_{\rm eff}$ (see the inset of Fig. 5). In the strongly perturbed regime, the chaotic effect significantly emerges and the main peak satisfies Eq. (8). In addition, the subpeak, which is attributed to the rejuvenation, is observed around the time necessary to stabilize the applied field, i.e., $t_{\rm s}\sim 100$ s. Under the perturbation with

TABLE I. The defenition of classification of our data under various perturbation conditions. (1) The condition $t_{\rm peak}=t_{\rm eff}+t_w$ is satisfied. (2) Subpeak is observed. (3) The condition $r\sim 1$ is satisfied. (4) The value of r attains the saturation value. For example, the data that belong to the *W* regime satisfy conditons (1) and (3), but do not satisfy (2) and (4).

Regime	(1)	(2)	(3)	(4)
W	Y	N	Y	N
WC	Y	N	N	N
SC	Y	Y	N	N
S	N	Y	N	Y

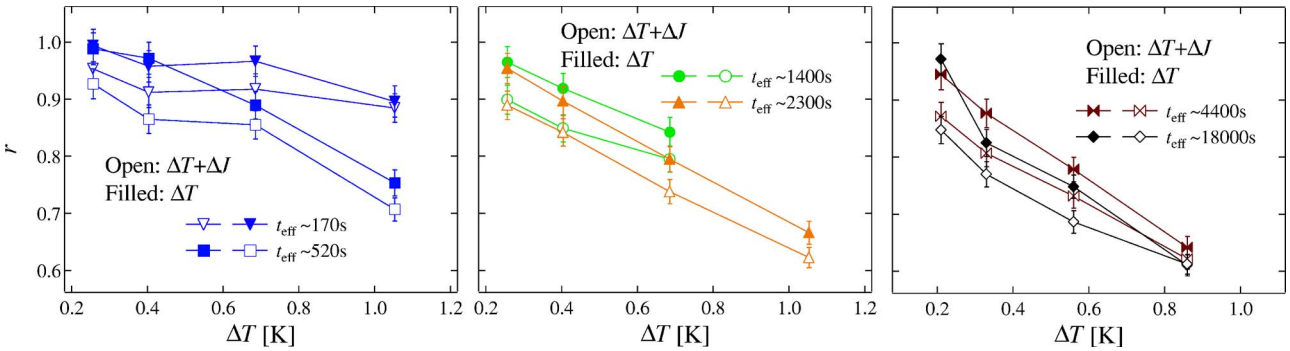

FIG. 6. (Color online) The ΔT-dependent r at various values of t_{eff}. Almost the same values of t_{eff} are gathered together in one graph. The left, middle, and right figures show r under $t_{\mathrm{eff}} \sim 170$ and 520 s, $t_{\mathrm{eff}} \sim 1400$ and 2300 s, and $t_{\mathrm{eff}} \sim 4400$ and 18000 s, respectively. The solid and open symbols show r under ΔT and $\Delta T + \Delta J$ perturbations, respectively.

$\Delta T = 1.05$ K, thus, the system at long t_{eff} may be in the S regime, where the order parameter ρ becomes saturated to a level common to both kinds of perturbations and the rejuvenation effect becomes noticeable. Except for the long t_{eff}, the system would not necessarily be classified into the S regime, because ρ is not saturated although the subpeak is observable. Therefore, this system may belong to the SC regime. The system at the shortest t_{eff} under ΔT perturbation is classified into the WC regime because of the absence of the subpeak.

At $\Delta T = 0.69$ K, t_{peak} almost merges into the reference curve except for the data at the longest $t_{\mathrm{eff}} + t_{\mathrm{w}}$. At the longest t_{eff}, however, the t_{peak} under the $\Delta T + \Delta J$ perturbation is shorter than that under the ΔT perturbation. Moreover, the subpeak appears under the $\Delta T + \Delta J$ perturbation only at the longest t_{eff} (see the inset of Fig. 4). Under both perturbations with $\Delta T = 0.69$ K, r rapidly decreases from 1 as t_{eff} increases, but does not become saturated (Fig. 5). Under the $\Delta T + \Delta J$ perturbation with $\Delta T = 0.69$ K, thus, the system at the longest t_{eff} gets into the SC regime, whereas it does not under the ΔT perturbation. Under the ΔT perturbation with $\Delta T = 0.69$ K, the system belongs to the WC regime except for the shortest observation time, at which it belongs to the W regime because r scarcely deviates from 1.

To clearly evaluate the overlap length under both the perturbations, r is abridged under the condition that t_{eff} be constant and ΔT is variable (Fig. 6). This mirrors the situation that the domain size grown during the perturbation stage is fixed while the overlap length $L_{\Delta T + (\Delta J)}$ is varied. At the shortest t_{eff} (~ 170 s) under the ΔT perturbation, r scarcely deviates from 1 as ΔT increases. This indicates that τ_{rec} is so short that the order parameter in ghost domains easily recovers. At long t_{eff}, r rapidly decreases as ΔT increases. This shows the crossover from the weakly to the strongly perturbed regimes through the decrease in the overlap length. The values of r are smaller under the $\Delta T + \Delta J$ perturbation than under the ΔT perturbation, but the difference in r between the perturbations becomes indistinct as ΔT increases. Ultimately it disappears at large ΔT due to the extremely long recovery time.

Figure 7 shows a schematic phase diagram in which the perturbation conditions are classified into the four regimes. In this figure, the boundary curves are guides to help the eyes grasp the qualitative aspect. As t_{eff} and ΔT increase, a systematic change from the W to the S regime is observed in the case of both the ΔT and $\Delta T + \Delta J$ perturbations. In Fig. 7, we find a feature in which the boundary curve in the $\Delta T + \Delta J$ perturbation data lies below the corresponding boundary curve in the ΔT perturbation data. This can be interpreted in terms of the decrease in the overlap length due to the additional perturbation ΔJ.

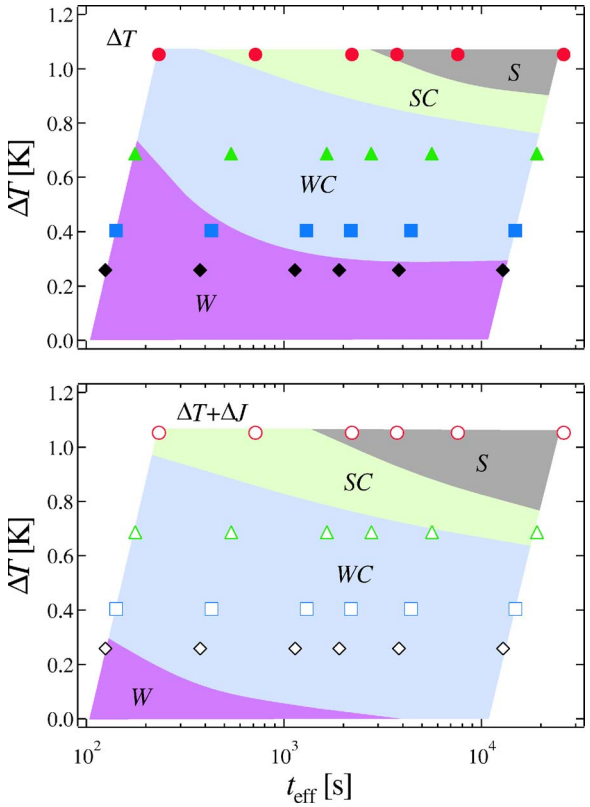

FIG. 7. (Color online) Schematic phase diagram where our data are classified into the four regimes: the weakly perturbed regime (W regime); the crossover regime, which is close to the weakly perturbed regime (WC regime); the crossover regime, which is close to the strongly perturbed regime (SC regime); the strongly perturbed regime (S regime) (bottom to top). The upper and lower figures show the diagram under ΔT and $\Delta T + \Delta J$ perturbations, respectively.

D. Effect of the bond perturbation

The order parameters under the $\Delta T+\Delta J$ perturbation are smaller than those under the ΔT perturbation with the same ΔT as mentioned above. These indicate that the ΔJ perturbation decreases the order parameter through the decrease in the overlap length. This is clearly demonstrated in Fig. 7 through the shift of boundary curves. The behavior of the subpeak, observed under both perturbations with $\Delta T=1.05$ K, suggests that the rejuvenation effect becomes pronounced due to the additional ΔJ, because the t'_{peak} is longer and r' is larger under the $\Delta T+\Delta J$ perturbation than under the ΔT perturbation [see the inset of Figs. 4(d) and 5].

In addition, we pay attention to the feature in which r under the $\Delta T+\Delta J$ perturbation with $\Delta T=0.26$ K is significantly smaller than 1 while r under the ΔT perturbation is practically equal to 1 as t_{eff} approaches zero, as shown in Fig. 5. This suggests that the ΔJ perturbation decreases the order parameter whereas the ΔT perturbation does not, even at infinitesimal t_{eff}. Thus, at $\Delta T=0.26$ K, the effect of the ΔT perturbation on the order parameter is so small that the ΔJ perturbation makes the dominant contribution. Based on the feature in which r under the $\Delta T+\Delta J$ perturbation with $\Delta T=0.26$ K is practically equal to that under the ΔT perturbation at $\Delta T=0.40$ K, we estimate that $\Delta J=0.14-0.40$ K at $\Delta T=0.26$ K.

V. CONCLUSION

The bond perturbation ΔJ, under photoillumination, affects the aging behavior of semiconductor spin glasses. We then estimated that $\Delta J\sim 0.14-0.40$ K at $\Delta T=0.26$ K. Thus, the bond perturbation ΔJ can significantly change the bond configuration, although the photoinduced magnetization in $Cd_{0.63}Mn_{0.37}Te$ is negligibly small.[28] This effect *cannot* be explained in terms of the strong separation of the time scales on different length scales. We attribute it to the decrease in the overlap length, i.e., $L_{\Delta T+\Delta J}<L_{\Delta T}$. Furthermore, we observed the crossover from weakly to strongly perturbed regimes in the bond cycling accompanied by the temperature cycling. These experimental results strongly suggest that "chaos" and the overlap length, which are the key concepts in the droplet picture, exist because the contribution of bond perturbation appears only in the overlap length.

In the future, it will be necessary to conduct a "pure" bond cycling experiment under photoillumination where there is no change in temperature. In addition, the mechanism of the bond perturbation using photoillumination should be clarified.

ACKNOWLEDGMENTS

This work was performed during the FY 2002 21st Century COE Program. We would like to thank S. Yabuuchi and Y. Oba for fruitful discussions.

[1] L. Lundgren, P. Svedlindh, P. Nordblad, and O. Beckman, Phys. Rev. Lett. **51**, 911 (1983).
[2] K. Jonason, E. Vincent, J. Hammann, J.-P. Bouchaud, and P. Nordblad, Phys. Rev. Lett. **81**, 3243 (1998).
[3] T. Jonsson, K. Jonason, P. Jönsson, and P. Nordblad, Phys. Rev. B **59**, 8770 (1999).
[4] D. S. Fisher and D. A. Huse, Phys. Rev. B **38**, 386 (1988).
[5] D. S. Fisher and D. A. Huse, Phys. Rev. B **38**, 373 (1988).
[6] A. J. Bray and M. A. Moore, Phys. Rev. Lett. **58**, 57 (1987).
[7] F. Scheffler, H. Yoshino, and P. Maass, Phys. Rev. B **68**, 060404(R) (2003).
[8] M. Sales and H. Yoshino, Phys. Rev. E **65**, 066131 (2002).
[9] P. E. Jönsson, H. Yoshino, and P. Nordblad, Phys. Rev. Lett. **90**, 059702 (2003).
[10] H. Yoshino, A. Lemaître, and J.-P. Bouchaud, Eur. Phys. J. B **20**, 367 (2001).
[11] H. Yoshino, J. Phys. A **36**, 10819 (2003).
[12] P. E. Jönsson, R. Mathieu, P. Nordblad, H. Yoshino, H. Aruga Katori, and A. Ito, Phys. Rev. B **70**, 174402 (2004).
[13] P. Nordblad, P. Svedlindh, L. Sandlund, and L. Lundgren, Phys. Lett. A **120**, 475 (1987).
[14] L. Sandlund, P. Svedlindh, P. Granberg, P. Nordblad, and L. Lundgren, J. Appl. Phys. **64**, 5616 (1988).
[15] P. Granberg, L. Lundgren, and P. Nordblad, J. Magn. Magn. Mater. **92**, 228 (1990).
[16] F. Bert, V. Dupuis, E. Vincent, J. Hammann, and J.-P. Bouchaud, Phys. Rev. Lett. **92**, 167203 (2004).
[17] M. Picco, F. Ricci-Tersenghi, and F. Ritort, Phys. Rev. B **63**, 174412 (2001).
[18] L. Berthier and J.-P. Bouchaud, Phys. Rev. B **66**, 054404 (2002).
[19] L. Berthier and A. P. Young, Phys. Rev. B **71**, 214429 (2005).
[20] J.-P. Bouchaud, V. Dupuis, J. Hammann, and E. Vincent, Phys. Rev. B **65**, 024439 (2002).
[21] L. Berthier and J.-P. Bouchaud, Phys. Rev. Lett. **90**, 059701 (2003).
[22] R. R. Galazka, S. Nagata, and P. H. Keesom, Phys. Rev. B **22**, 3344 (1980).
[23] P. Nordblad, P. Svedlindh, J. Ferré, and M. Ayadi, J. Magn. Magn. Mater. **59**, 250 (1986).
[24] A. Mauger, J. Ferré, M. Ayadi, and P. Nordblad, Phys. Rev. B **37**, 9022 (1988); A. Mauger, J. Ferré, and P. Beauvillain, *ibid.* **40**, 862 (1989).
[25] Y. Zhou, C. Rigaux, A. Mycielski, M. Menant, and N. Bontemps, Phys. Rev. B **40**, 8111 (1989).
[26] M. Smith, A. Dissanayake, and H. X. Jiang, Phys. Rev. B **49**, 4514 (1994).
[27] T. Sato and A. Hori, J. Magn. Magn. Mater. **272–276**, 1337 (2004).
[28] H. Kawai and T. Sato, J. Appl. Phys. **85**, 7310 (1999).
[29] As shown in Fig. 1, the FC susceptibility increases as temperature decreases, which is different from the conventional spin-glass behavior. This is attributed to the paramagnetic contribution from the small magnetic clusters, which are not belonging to the freezing spins. See Ref. 22.
[30] The typical spin-flip time τ_0 in spin glasses has been evaluated as $\sim 10^{-13}$ s, e.g., $10^{-12}-10^{-14}$ s for $Cd_{0.6}Mn_{0.4}Te$ and

10^{-12}–10^{-15} s for $Cd_{0.55}Mn_{0.45}Te$ are evaluated [see A. Mauger, J. Ferre, M. Ayadi, and P. Nordblad, Phys. Rev. B **37**, 9022 (1988) and M. Saint-Paul, J. L. Tholence, and W. Giriat, Solid State Commun. **60**, 621 (1986)]. The duration of the perturbation is insensitive to the value of τ_0, and we assume the typical spin-flip time of 10^{-13} s in the present work.

[31] P. Granberg, L. Sandlund, P. Nordblad, P. Svedlindh, and L. Lundgren, Phys. Rev. B **38**, 7097 (1988).